Velocity inversion in nanochannel flow

Youngkyun Jung
Supercomputing Center, Korea Institute of Science and Technology Information, P.O. Box 122, Yuseong-gu, Daejeon 305-806, Korea
(Received 11 September 2006; published 18 May 2007)

The nanoscale cylindrical Couette flow is investigated by means of molecular dynamics simulations, in the case where the inner cylinder is rotating whereas the outer cylinder is at rest. We find that the tangential velocity of the flow is inverted when the fluid-wall interaction near the outer cylinder is weak and the fluid density is low. The unusual velocity inversion behavior is shown to be strongly related to the degree of the slip between the fluid and the outer cylinder, which is determined by the presence or absence of the layering of the fluid near the outer wall.

DOI: 10.1103/PhysRevE.75.051203 PACS number(s): 61.20.Ja, 83.50.Ha, 83.50.Lh, 83.50.Rp

I. INTRODUCTION

Couette flow between two concentric rotating cylinders shows interesting and unexpected features such as "velocity inversion" which implies that the tangential velocity of the flow increases with distance from a rotating cylinder to a stationary cylinder. The velocity inversion phenomenon has been studied with analytical and numerical methods. Einzel *et al.* [1] first predicted by suggesting a generalized slip boundary condition for incompressible flow over curved or rough surfaces that the velocity profile would become inverted in the case of large velocity slip at the wall surfaces. Tibbs *et al.* [2] and Aoki *et al.* [3] confirmed the prediction of the anomalous behavior using direct simulation Monte Carlo calculations and some analytic approaches and found that the values of the accommodation coefficients in their models play an important role in the velocity inversion phenomenon. In all those studies, they found that the velocity inversion phenomenon only occurred for a large velocity slip at a small value of the accommodation coefficient. The accommodation coefficient is an important parameter in determining the degree of slip of the fluid at the wall and represents the average tangential momentum exchange between the flowing fluid particles and the wall boundary. The case of zero value of the coefficient is called specular reflection, meaning zero friction. When its value is unity, the reflection is diffuse, meaning that the fluid particles are reflected with zero average tangential velocity. Recently, similar studies for the velocity inversion phenomenon were performed [4–6]. It, however, is difficult that the concept of an accommodation coefficient can apply to all types of fluids or the nature of the wall materials.

Molecular dynamics (MD) is a very powerful tool in the exploration and study of the nature of the flow at the boundaries independent of the properties of the fluid and wall materials. For simple Lennard-Jones liquids, the wetting properties of the fluid can be modeled by wetting parameter varying the strength of the fluid-wall attraction [7–9]. The wetting parameter could directly be related to the accommodation coefficient of the fluid-wall system. When the value of the parameter is zero (nonwetting or specular reflective), the fluid-wall interface is specular reflective similar to the case of zero value of the accommodation coefficient. When it is unity (wetting or attractive), the surface is diffuse reflection. The large slip at the fluid-wall interface exhibits under nonwetting condition and it decreases as the value of the wetting parameter increases to unity. The degree of the slip is also dependent on the density of the fluid. Even at a strongly attractive wall, a large slip was found in the highly dilute gas regime [9].

In this paper we use MD simulations for Lennard-Jones liquids to investigate the velocity inversion phenomenon in nanoscale cylindrical Couette flows of the concentric rotating cylinders, varying the fluid density and the value of the wetting parameter. The tangential velocity of the flow is measured in the case where the inner cylinder is rotating whereas the outer cylinder is at rest. At low fluid density and under the poor wetting condition, the velocity is inverted with a large velocity slip near the outer cylinder. On the other hand, at high density or under the good wetting condition, such inversion does not occur with the layer adsorption of the fluid near the outer cylinder. Next, the radial force field is considered, and it is found that the radial force is a better measurement than the fluid density to examine the effect of the layering near the outer cylinder on the velocity slip.

II. MOLECULAR DYNAMICS SIMULATIONS

To investigate the properties of the nanochannel flows in a curved surface, we have conducted MD simulations of the cylindrical Couette flows in the concentric rotating cylinders as shown in Fig. 1. Standard MD techniques are used [10,11]. The fluid particles and the wall particles at a distance r interact through a Lennard-Jones (LJ) potential, $V_{ij}(r)=4\epsilon[(r/\sigma)^{-12}-A_{ij}(r/\sigma)^{-6}]$, where ϵ and σ represent the

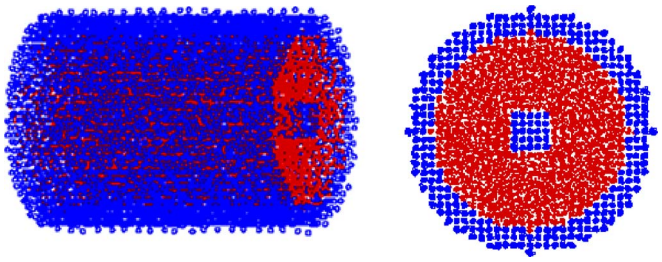

FIG. 1. (Color online) Views of a fluid in a nanochannel consisting of two concentric cylinders.

energy and length scales, and $A_{ij}=A_{ji}$ is a dimensionless parameter that controls the attractive part of the potential for the fluid-fluid and the fluid-wall particles. As mentioned previously, this parameter is similar to the accommodation coefficient in continuum descriptions [1–6]. The potential is truncated at $r_c=2.5\sigma$. Newton's equations are integrated with a velocity Verlet algorithm [11] with a time step $\delta t=0.005\tau$, where $\tau=\sigma(m/\epsilon)^{1/2}$ represents the characteristic time scale with fluid particle mass m. A dissipative particle dynamics (DPD) thermostat [12] is used to keep the system at a constant temperature $T=1.0\epsilon/k_B$, where k_B is the Boltzmann constant. A coupling constant and a weight function are chosen to be $\zeta=0.5\tau^{-1}$ and $w(r_{ij})=1-\frac{r_{ij}}{r_c}$, respectively, with the same cutoff $r_c=2.5\sigma$ as the LJ potential (for further details see Ref. [12]). A Langevin thermostat [13] is also considered to check the correctness of our results. The thermostat with damping constant $0.1\tau^{-1}$ is only applied in the axial direction of the cylinder in which the fluid is not being sheared. We have checked that both thermostats give consistent results confirming the appearance of the velocity inversion phenomenon in our system. Thus, in this paper, we only present results obtained with the DPD thermostat.

The fluids are confined to a gap between two concentric cylinders, whose walls are composed of particles of mass $m_w=100m$, tethered by a stiff linear spring with constant $k_w=100$ to fixed lattice sites. The fluid particles interact via the LJ potential with the $A_{ff}=1$. The channel walls are made of the same material as the particle and interact with fluid particles with $A_{fw}=1$ at the inner cylinder and $A_{fw}=0$ at the outer cylinder. The periodic boundary condition is used in the axial direction. All simulations are performed with a fixed inner cylinder radius as $R_i/\sigma=2.05$ (4 molecular diameters) and different radii of the outer cylinder ranging from 10.26 (20 molecular diameters) to 27.36 (53 molecular diameters).

III. NUMERICAL RESULTS AND DISCUSSION

A. Density and tangential velocity profiles

The fluid is sheared by rotating the inner cylinder at a constant angular velocity $\omega=0.1$ rad/τ, while the outer cylinder remains stationary for all the simulations. After an equilibration time of $5\times10^4\tau$, the averages are obtained by dividing the interior of the tube into cylindrical shells of thickness $\sigma/4$ for a period of about $2\times10^5\tau$. Figure 2 shows the density profiles for both the stationary ($\omega=0.0$ rad/τ) and the rotating ($\omega=0.1$ rad/τ) inner cylinders denoted by the blue dashed and the red solid line, respectively. The fluid densities used in Fig. 2 which are volume-average number densities of the fluids, ρ/σ^3, are 0.04, 0.40, 0.52, and 0.82. There are fluid layers near the inner cylinder corresponding to density peaks as a consequence of the attractive interaction ($A_{fw}=1$) between the fluid particles and the inner cylinder, while near the outer cylinder with $A_{fw}=0$ the peak does not exist except for the dense regime [see Fig. 2(d)]. For the dense regime, however, a large number of layers are observed near the outer cylinder due to the high packing of the particles. When the inner cylinder is rotated, the angular momentum attained from the rotating cylinder is continuously transferred to the outer region through the interparticle interactions, so that the particles near the inner cylinder are pushed out to the outer region.

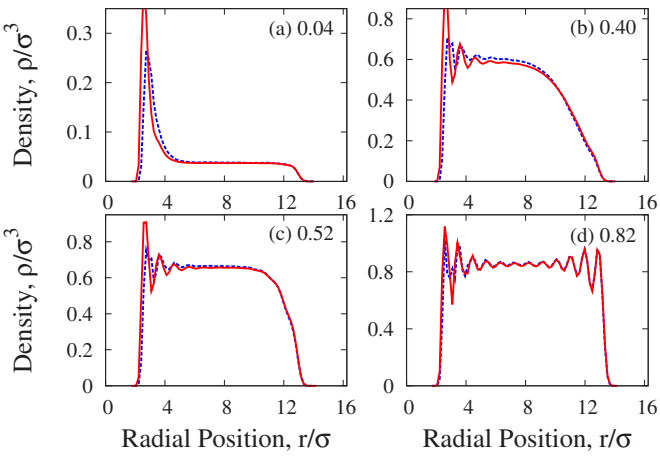

FIG. 2. (Color online) Density profiles for the angular velocities $\omega=0.0$ rad/τ (blue dotted line) and $\omega=0.1$ rad/τ (red solid line) with different fluid densities 0.04, 0.40, 0.52, and 0.82.

We have carried out the simulations at different fluid densities ranging from 0.04 to 0.82 to measure the tangential velocity of the flows. The tangential velocity initially decreases with the radial position due to the momentum dissipation through interparticle interactions as shown in Fig. 3. It, however, is shown that the velocities are inverted at below a certain fluid density of about $\rho/\sigma^3\approx0.6$. In other words, the velocity increases with distance from the rotating inner cylinder. This unusual behavior of the tangential velocity is similar to the results of the previous studies [1–5]. The velocities finally become decaying again near the outer cylinder, which will be explained in detail below. It is well-known that the slip velocity at the stationary outer cylinder plays a crucial role in the velocity inversion [1]. In our simulations such slip velocity appear at below a certain fluid density

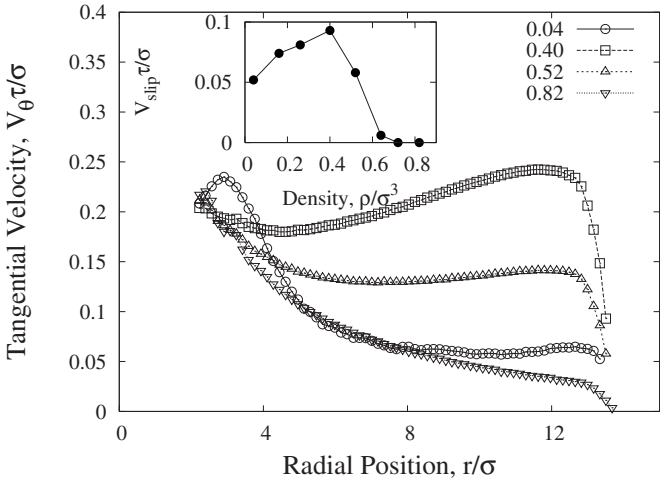

FIG. 3. Tangential velocities of the flows as a function of the radial positions at different volume-average number densities of the fluids. The inset shows the slip velocities, which are measured at the closest bin to the outer cylinder, as a function of the fluid density.

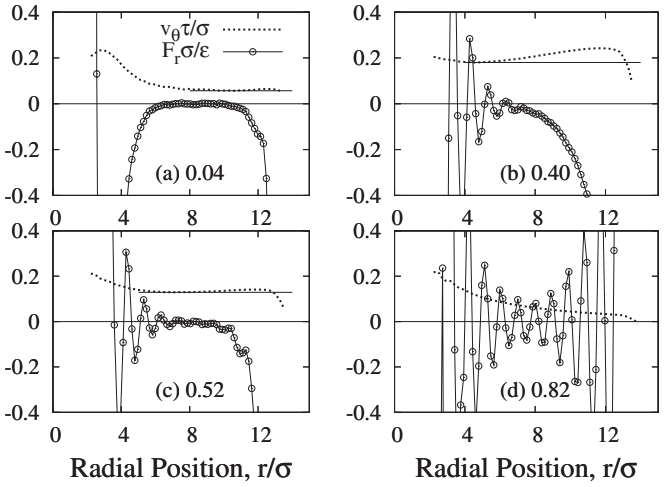

FIG. 4. Radial force profiles of the flow (circle) for the indicated values of the fluid density ρ/σ^3 (0.04, 0.40, 0.52, and 0.82) as a function of the radial position at $\omega=0.1$ rad/τ. The tangential velocity (dotted line) profiles in Fig. 3 are added to compare them with the radial force profiles. The horizontal solid lines are used as guidelines to the eye.

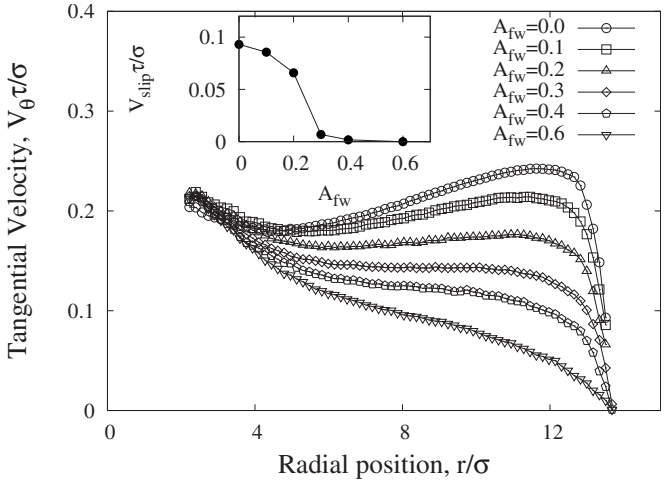

FIG. 5. Tangential velocity profiles with different A_{fw} ranging from 0.0 to 0.6. The fluid density is fixed at $\rho/\sigma^3=0.40$. The inset shows the slip velocity near the stationary outer cylinder as a function of A_{fw}.

$\rho/\sigma^3\approx 0.6$, below which the velocities are inverted. Above 0.6, no velocity slips and no tangential velocity is inverted even though the fluid-wall interaction is specular ($A_{fw}=0$). The inset of Fig. 3 shows the slip velocity near the outer cylinder as a function of the fluid density. The maximum value of the slip velocity is located at $\rho/\sigma^3=0.40$, where the degree of the velocity inversion is largest. For low density, the slip velocity increases with fluid density where the interactions of the particles with the wall and with each other are dominant. However, for dense cases, it decreases where viscosity becomes dominant, so that the flow gets slowed down. It is certain that the velocity inversions are shown if the slip velocity is higher than a certain value.

B. Radial force profile

In order to gain an insight into such an unusual inverted velocity profile in the case of a stationary outer cylinder and a rotating inner cylinder, we measure the radial force generated by both the rotating inner cylinder with $A_{fw}=1$ and the stationary outer cylinder with $A_{fw}=0$. Figure 4 shows the radial force profiles at different fluid densities, corresponding to 0.04, 0.40, 0.52, and 0.82. The tangential velocity profiles in Fig. 3 are added to compare them with the radial force profiles. It is important to put our finger on the appearance of the peaks in the radial force profiles, as in the density profiles (see Fig. 2). However, compared to the peaks of the density, the oscillations of the radial force are shown more clearly. In the vicinity of the inner cylinder, oscillations of the radial force are revealed due to the adsorption of the fluid at the cylinder. On the other hand, near the reflective outer cylinder there exist no such oscillation except for the dense regime as in Fig. 4(d). In Figs. 4(a)–4(c), there is a point at which the outward motion of the fluid meets the inward motion, which results from the competition between the centrifugal force by the rotating inner cylinder and the centripetal force by the reflective outer cylinder. Moreover, due to the lack of fluid-wall interaction near the outer cylinder, the angular momentum attained from the rotating inner cylinder is well-transferred to the outer region and induces the velocity slip. It is interesting to note that the tangential velocity begins to be inverted at the point. However, there is no such point for the dense case as shown in Fig. 4(d). In this regime, the fluid-wall interaction near the outer cylinder is very strong, so that the fluids in the first layer can hardly slip and the first fluid layer induces a second layer by the fluid-fluid interaction. The second layer induces a third, and so on. Based on these observations, it is certain that the presence of the layering in the vicinity of the outer cylinder is a key factor to determine whether the velocity inversion phenomenon appears or not.

C. Layering effect

To understand the effect of the layering near the outer cylinder on the velocity inversion phenomenon, we measure the tangential velocity with different values of interaction parameter A_{fw} between the fluid and the outer cylinder at fixed fluid density $\rho/\sigma^3=0.4$. At this density, the velocity inversion behavior can be seen most clearly (see Fig. 3). As A_{fw} increases, the degree of the velocity inversion gradually decreases and finally disappears at exceeding $A_{fw}=0.3$ as shown in Fig. 5. The slip velocity shown in the inset of Fig. 5 for six independent realizations of different A_{fw}, corresponding to 0.0, 0.1, 0.2, 0.3, 0.4, and 0.6, also decreases to zero. These indicate that the velocity inversion behavior is strongly related to the strength of the fluid-wall interaction near the outer cylinder. The responses of the density and the radial force with increasing the value of A_{fw} is shown in Fig. 6. As the value of A_{fw} increases, the outer cylinder becomes more attractive so that more fluid particles can move to the outer region and the adsorbed layers begin to form near the outer cylinder. This formation of the adsorbed layers can be seen most clearly in the radial force profile rather than in the

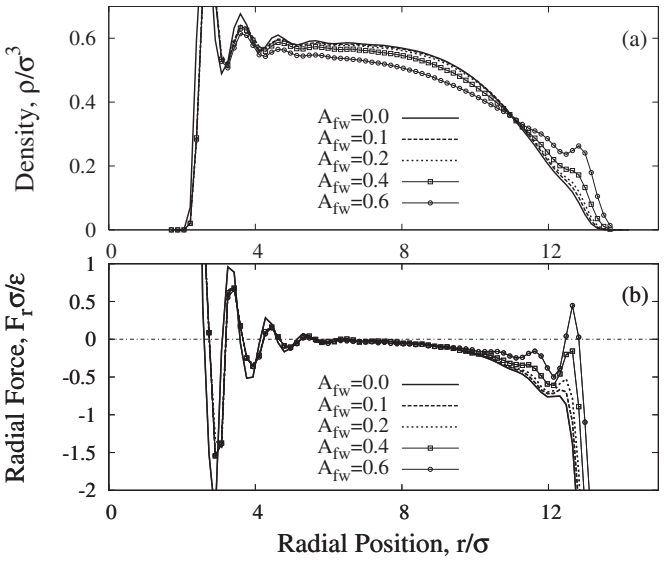

FIG. 6. Density (a) and radial force (b) profiles of the flows as a function of the radial position at $\omega=0.1$ rad/τ with several values of A_{fw}. The fluid density is fixed at $\rho/\sigma^3=0.40$. The dotted line in (b) denotes a zero value of the radial force at which the sign of the radial force is changed.

density profile as revealed in Fig. 6. Even for $A_{fw}=0.0$, an indication of a peak of the radial force is shown. The fluid particles of the first layer almost stick to the wall, which causes the flow to retard in the vicinity of the wall. The rapid decay of the tangential velocity near the outer cylinder shown in Fig. 5 can be explained by this layering effect even though it is weak. When the value of A_{fw} is small (less than 0.3), the first layer adsorption only appeared weakly and its size gradually increases as A_{fw} increases from zero. For a small value of A_{fw}, the velocity of the flow can largely slip and the velocity can be inverted. As A_{fw} increases beyond 0.3, the effect of the first layer is getting strong and induces a second layer, the second layer induces a third layer, and so on. From the layer adsorption point of view, the fluid particles of a second layer are retarded by the first layer, a third layer is retarded by the second layer, and so on. As the number of fluid layer increases, the no-slip nature at the fluid-wall interface spreads into the bulk, so that the flow cannot slip and no velocity inversion appears. It is finally concluded that the appearance of the velocity inversion phenomenon is determined by whether the layer adsorption near the outer cylinder is present or not.

The response of the velocity inversion with increasing the radius of the outer cylinder ranging from $R/\sigma=10.26$ to 27.36 at fixed fluid density 0.40 and angular velocity 0.1 rad/τ is shown in Fig. 7. At $R/\sigma=10.26$, the tangential velocity is fully inverted. As the radius of the outer cylinder increases, the effect of the rotating cylinder is reduced, so that finally the velocity would not slip any more and not be inverted at a given angular velocity. We find also that no inverted velocity profile appears in the case where the inner cylinder is stationary whereas the outer cylinder is rotating.

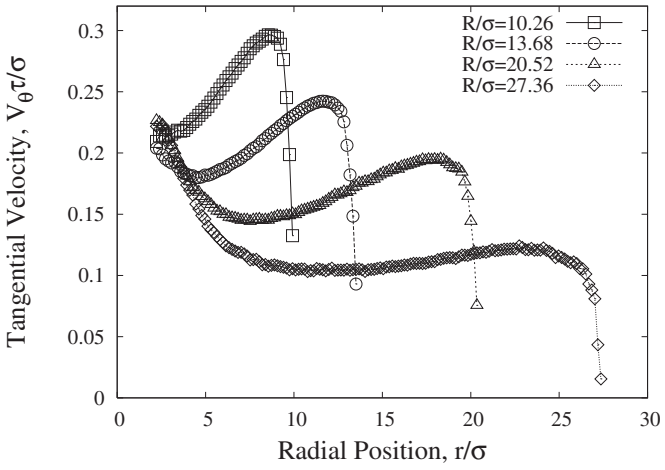

FIG. 7. Tangential velocity profiles with four different radii of the outer cylinders at given fluid density $\rho/\sigma^3=0.40$ and fixed angular velocity $\omega=0.1$ rad/τ.

IV. CONCLUSIONS

Using molecular dynamics simulation, we study the behavior of the nanoscale cylindrical Couette flow between two concentric rotating cylinders. In simulations, both DPD and Langevin thermostats which are suitable for out-of-equilibrium simulations are used to keep the system at a constant temperature. When the inner cylinder rotates and the outer cylinder is at rest, we find that the tangential velocity is inverted with a large velocity slip at the outer cylinder. The large slip at the outer cylinder, which plays an important role in the appearance of the inversion, occurs at low fluid density and weak fluid-wall interaction near the outer cylinder. We also find that the appearance of the inversion behavior is strongly related to the presence or absence of the layering of the fluid near the outer cylinder. The formation of the layers can be seen most clearly in the radial force profile.

ACKNOWLEDGMENTS

The author would like to thank Jysoo Lee for useful discussions. This work was supported in part by a research fund from IBM KOREA.

[1] D. Einzel, P. Panzer, and M. Liu, Phys. Rev. Lett. **64**, 2269 (1990).
[2] K. W. Tibbs, F. Baras, and A. L. Garcia, Phys. Rev. E **56**, 2282 (1997).
[3] K. Aoki, H. Yoshida, T. Nakanishi, and A. L. Garcia, Phys. Rev. E **68**, 016302 (2003).
[4] D. A. Lockerby, J. M. Reese, D. R. Emerson, and R. W. Barber, Phys. Rev. E **70**, 017303 (2004).
[5] S. Yuhong, R. W. Barber, and D. R. Emerson, Phys. Fluids **17**, 047102 (2005).

[6] R. S. Myong, J. M. Reese, R. W. Barber, and D. R. Emerson, Phys. Fluids **17**, 087105 (2005).
[7] J.-L. Barrat and L. Bocquet, Phys. Rev. Lett. **82**, 4671 (1999).
[8] M. Cieplak, J. Koplik, and J. R. Banavar, Physica A **284**, 281 (1999); **287**, 153 (2000).
[9] M. Cieplak, J. Koplik, and J. R. Banavar, Phys. Rev. Lett. **86**, 803 (2001).
[10] G. Drazer, B. Khusid, and J. Koplik, Phys. Fluids **17**, 017102 (2005).
[11] M. P. Allen and D. J. Tildesley, *Computer Simulation of Liquids* (Clarendon, Oxford, 1987).
[12] T. Soddemann, B. Dünweg, and K. Kremer, Phys. Rev. E **68**, 046702 (2003).
[13] G. S. Grest and K. Kremer, Phys. Rev. A **33**, 3628 (1986).